

Article

Single-Atom Alloy Pd₁Ag₁₀/CeO₂-ZrO₂ as a Promising Catalyst for Selective Alkyne Hydrogenation

Pavel V. Markov¹, Galina O. Bragina¹, Nadezhda S. Smirnova¹, Galina N. Baeva¹, Igor S. Mashkovsky^{1,*}, Evgeny Y. Gerasimov², Andrey V. Bukhtiyarov², Yan. V. Zubavichus² and Alexander Y. Stakheev^{1,*}

¹ N. D. Zelinsky Institute of Organic Chemistry RAS, Leninsky Prospect 47, 119991 Moscow, Russia

² G. K. Boreskov Institute of Catalysis, Siberian Branch of the Russian Academy of Sciences, Academician Lavrentiev Prospect 5, 630090 Novosibirsk, Russia

* Correspondence: im@ioc.ac.ru (I.S.M.); st@ioc.ac.ru (A.Y.S.)

Abstract: The effect of support on the performance of Pd₁Ag₁₀/Al₂O₃ and Pd₁Ag₁₀/CeO₂-ZrO₂ catalysts in the selective hydrogenation of diphenylacetylene (DPA) was studied. Characterization of the catalyst by DRIFTS-CO and HRTEM revealed the formation of a PdAg single-atom alloy (SAA) structure on the surface of PdAg nanoparticles, with Pd₁ sites isolated by Ag atoms. It was found that the use of CeO₂-ZrO₂ as a carrier makes it possible to increase the activity of the Pd₁Ag₁₀ catalyst by a factor of three without loss of selectivity compared to the reference Pd₁Ag₁₀/Al₂O₃. According to the HRTEM data, this catalytic behavior can be explained by an increase in the dispersion of Pd₁Ag₁₀/CeO₂-ZrO₂ compared to its Pd₁Ag₁₀/Al₂O₃ counterpart. As evidenced by DRIFTS-CO data, the high selectivity of the Pd₁Ag₁₀/CeO₂-ZrO₂ sample presumably stems from the stability of the structure of isolated Pd₁ sites on the surface of SAA Pd₁Ag₁₀/CeO₂-ZrO₂.

Keywords: single-atom alloy catalyst; isolated Pd₁ sites; liquid-phase hydrogenation; alkynes; diphenylacetylene; cerium-zirconium carrier; palladium-silver



Citation: Markov, P.V.; Bragina, G.O.; Smirnova, N.S.; Baeva, G.N.; Mashkovsky, I.S.; Gerasimov, E.Y.; Bukhtiyarov, A.V.; Zubavichus, Y.V.; Stakheev, A.Y. Single-Atom Alloy Pd₁Ag₁₀/CeO₂-ZrO₂ as a Promising Catalyst for Selective Alkyne Hydrogenation. *Inorganics* **2023**, *11*, 150. <https://doi.org/10.3390/inorganics11040150>

Academic Editor: Duncan H. Gregory

Received: 8 March 2023

Revised: 24 March 2023

Accepted: 29 March 2023

Published: 1 April 2023



Copyright: © 2023 by the authors. Licensee MDPI, Basel, Switzerland. This article is an open access article distributed under the terms and conditions of the Creative Commons Attribution (CC BY) license (<https://creativecommons.org/licenses/by/4.0/>).

1. Introduction

Supported metal catalysts based on noble metals (Pd, Pt, Rh, Ir) are among the most common heterogeneous catalysts [1–4]. Since they are highly active, thermally stable and easy to separate from the reaction mixture, they are widely used both in industry and in laboratory practice. Thus, supported palladium catalysts are widely used in the selective hydrogenation of alkynes [5–7]. A typical example is the large-scale removal of acetylene impurities from pyrolysis ethylene before its polymerization. An important reaction is also the purification of styrene from trace amounts of phenylacetylene in the production of polystyrene, since even insignificant concentrations of alkynes poison metallocene polymerization catalysts. It should also be noted that the selective hydrogenation of substituted alkynes is one of the key routes in the synthesis of many complex alkene compounds, since it can be performed with high stereoselectivity [8,9].

A significant drawback of heterogeneous metal-supported catalysts is their lower selectivity compared to homogeneous metal-complex catalysts. The high inhomogeneity of active sites is one of the key factors that largely determine the catalytic performances in terms of activity and selectivity [10]. In the last decade, the methodology of single-atom alloys (SAAs) has been successfully used to improve the selectivity of hydrogenation catalysts [11–14]. Typically, they are catalytic systems with single atoms of a catalytically active metal (Pd, Pt) alloyed into the surface of a host metal (usually Au, Ag, In, Zn), whose hydrogenation activity is negligible. Such a structure leads to the formation of active sites with identical adsorption and catalytic characteristics, which makes it possible to obtain target products with extremely high selectivity. Thus, several authors reported on the preparation of efficient SAA Pd-based catalysts for the selective hydrogenation of styrene,

butadiene and acetylene, as well as in the dehydrogenation of acetic acid [15–21]. Despite the high selectivity of SAA catalysts toward the desired products, their activity is usually limited owing to the small number of isolated Pd sites on the surface of PdM nanoparticles. Hence, the development of a method for improving their catalytic activity is an urgent task.

The activity of the catalyst can be significantly affected by the support [22–24]. Its choice is usually determined by the degree of interaction of metal nanoparticles with the surface. The strong interaction of the support with the deposited metal particles can provoke a change in their electronic state and enhance their dispersion [7,25]. The use of cerium oxide as a support makes it possible to significantly (3–5-fold) increase the catalytic activity in a number of reactions [24], although the reasons for the change in catalytic activity still remain unclear. As reported earlier for the hydrogenation of phenol to cyclohexanone, an increase in the catalytic activity of the Pd/CeO₂ catalyst can be facilitated by an increase in the dispersion of Pd [26,27].

It should be noted that the structural and textural characteristics of CeO₂ can be significantly improved by using ZrO₂ as a modifier. Even small amounts of ZrO₂ can increase the thermal stability of CeO₂ through the formation of a CeO₂–ZrO₂ substitutional solid solution [28,29]. Moreover, the increase in the activity of monometallic M/CeO₂–ZrO₂ (M = Pt, Pd) catalysts was observed in the hydrogenation of nitroaromatics and carbonyl compounds [30–36]. The authors suggested that the high catalytic activity of the Pt/CeO₂–ZrO₂ catalyst may be due to H₂ spillover that provokes the formation of adsorption and activation centers of the initial substrate as a result of the partial reduction of CeO₂–ZrO₂ [33–36].

However, reported examples illustrate the increase in activity for monometallic catalysts only. To the best of our knowledge, the literature completely lacks data on the improvement of the performance of SAA catalysts on Ce-containing supports. With this in mind, the aim of the current work was to study the effect of a CeO₂–ZrO₂ carrier on the performance of a PdAg single-atom alloy catalyst in diphenylacetylene (DPA) hydrogenation with special attention paid to the selectivity of the catalyst. PdAg₁₀/Al₂O₃ was used as the reference catalyst. The catalysts were designated as PdAg₁₀/CZ and PdAg₁₀/A.

Note that one of the efficient ways to control the composition of active sites and, as a consequence, the catalytic performance of single-atom catalysts is to determine the optimal ratio of active and inactive components in its structure. Our previous studies demonstrated significant enhancement of the selectivity in partial alkyne hydrogenation for PdAg/Al₂O₃ when using a Pd:Ag ratio of 1:1–1:5 [37–39]. Here, we focused on catalysts with a Pd:Ag molar ratio of 1:10. Their structural characteristics were studied using DRIFT spectroscopy of adsorbed CO and transmission high-resolution electron microscopy.

2. Results and Discussion

2.1. Mapping Transmission Electron Microscopy

The morphology, phase composition and particle size of the PdAg₁₀ catalysts were obtained using HRTEM. Figure 1 represents the HAADF STEM micrograph (a) and EDX mapping (b) of a PdAg₁₀/CZ catalyst. A narrow particle size distribution was observed with an average particle size of 4.4 nm (Figure 1a). The sample contained rounded particles uniformly distributed on the support surface with no highly enriched areas. The phase composition of the particles was determined from the EDX mapping. The data obtained indicate that the bimetallic particles are PdAg₁₀, which is close to the initial stoichiometry (see Figure S1a and Table S1).

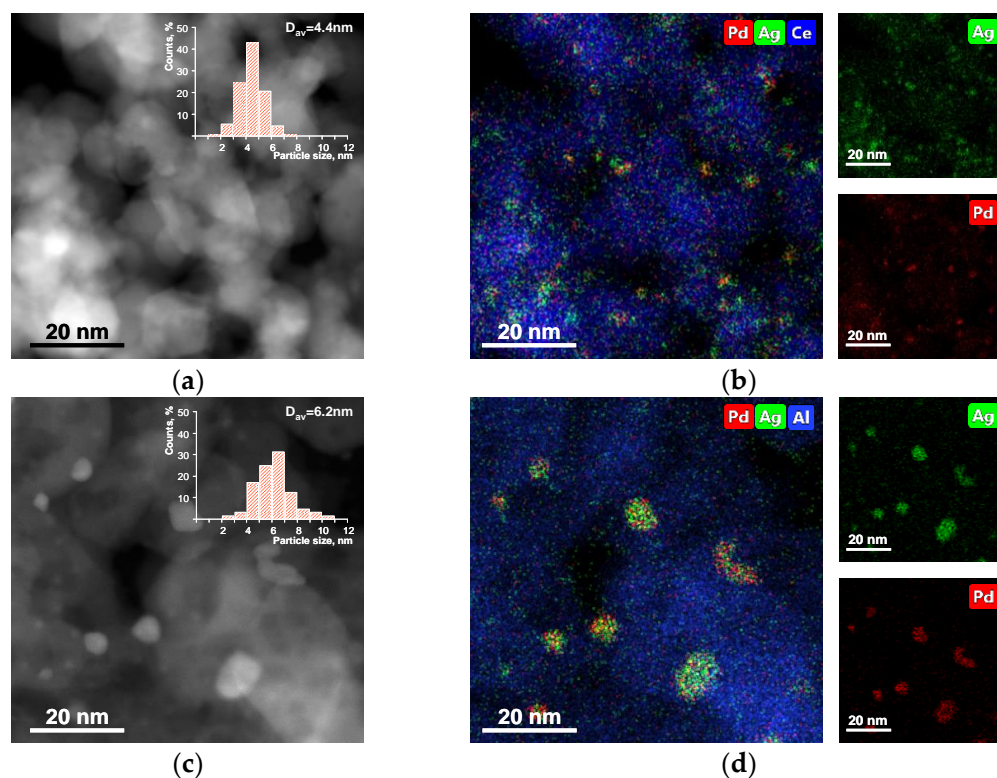


Figure 1. HAADF STEM microphotography and HAADF STEM-mode EDX mapping of PdAg₁₀/CZ (a,b) and PdAg₁₀/A (c,d) catalysts. Inserts in Figure 1a,c represent the corresponding particle-size distribution histograms.

For the PdAg₁₀/A catalyst, a wider particle size distribution (from 2 to 12 nm) was detected with an average size of 6.2 nm (Figure 1c). This catalyst also contained rounded particles with a uniform distribution on the catalyst surface. The EDX study revealed the formation of PdAg nanoparticles for SAA PdAg₁₀/A catalyst with Pd/Ag close to the stoichiometric 1/10 molar ratio (see Figure S1b and Table S2).

2.2. DRIFT Spectroscopy of Adsorbed CO (DRIFTS-CO)

The surface structure of *in situ* reduced catalysts was studied via the DRIFT spectroscopy of adsorbed CO (Figure 2), which is known as a powerful tool for the analysis of SAA [40,41].

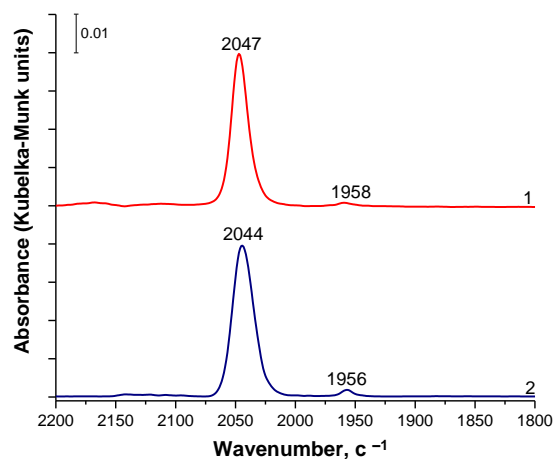


Figure 2. DRIFT spectra of adsorbed CO for the PdAg₁₀/A (1) and PdAg₁₀/CZ (2) catalysts.

The DRIFTS-CO spectra of the freshly reduced PdAg₁₀/A and PdAg₁₀/CZ samples are very close to each other, indicating the similarity of their surface structure. Both spectra are characterized by the presence of an intensive symmetric absorption band centered at 2044–2047 cm⁻¹, characteristic of linearly adsorbed CO on the Pd atoms. The negligible intensity of the signal in the wavenumber range of 2000–1800 cm⁻¹ confirms practically complete absence of multipoint CO adsorption on the Pd-Ag surface. This indicates the disappearance of multiatomic Pd_n surface sites ($n \geq 2$) with the formation of a Pd-Ag SAA structure where Pd₁ atoms are separated from each other by Ag atoms [42–45].

Formation of Pd-Ag nanoparticles provokes a redistribution of the electron density between Pd and Ag atoms, which leads to the donation of electron density to the antibonding π -orbital of the adsorbed CO with the C=O bond subsequently weakening [46]. This effect results in a shift of the linear CO band toward lower wavenumbers (~2040–2050 cm⁻¹) compared to the spectrum of monometallic Pd (~2080–2090 cm⁻¹) [47]. Note that both the small width and the symmetry of the band of linearly adsorbed CO points to the formation of highly homogeneous Pd₁ active sites.

2.3. Catalytic Tests

Figure 3a,b compare the product distribution of diphenylacetylene (DPA) hydrogenation as a function of the reaction time for the reference PdAg₁₀/A sample and the PdAg₁₀/CZ catalyst. It is evident that, over both catalysts, the reaction proceeds via a two-step sequential scheme (Figure 4). According to this scheme, DPA hydrogenation to *cis*- (route *a*) and *trans*-diphenylethylene (DPE) (route *b*) first occurred (first step) followed by the alkenes' hydrogenation to diphenylethane (DPEt) (second step) via routes *f* and *e*. It should be noted that *trans*-DPE formation is also possible through hydro-isomerization (route *d*) [48,49].

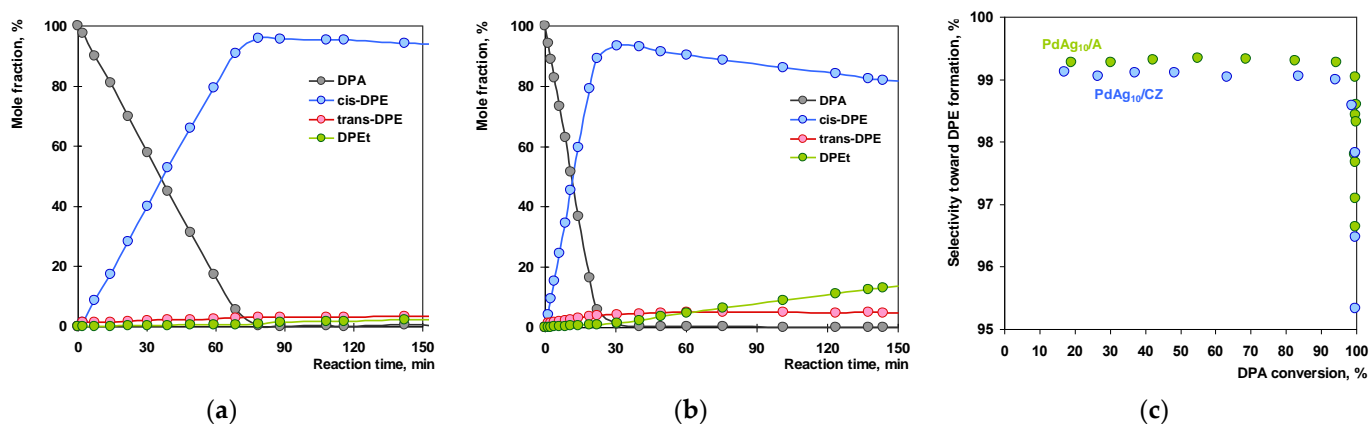


Figure 3. DPA hydrogenation products distribution over PdAg₁₀/A (a) and PdAg₁₀/CZ (b) catalysts based on chromatographic analysis data; (c) dependence of selectivity toward stilbene formation. $P(\text{H}_2) = 5$ bar, $m_{\text{cat}} = 10$ mg, $[\text{DPA}] = 1$ mmol.

Figure 3 clearly shows the considerable differences in the DPA hydrogenation rates over SAA PdAg₁₀/A and PdAg₁₀/CZ catalysts. Thus, the DPA conversion over the reference PdAg₁₀/A was completed in 80 min, while over the PdAg₁₀/CZ, sample it took 30 min. Calculation of the GC data shows that the rate of DPA to DPE hydrogenation (r_1) over PdAg₁₀/CZ was 3.1 times higher than that over the reference PdAg₁₀/A catalysts: 4.21 and 1.36 mmol DPA min⁻¹ g_{cat}⁻¹, respectively (see Table 1). This observation is in agreement with the recent literature data on the positive effect of Ce-Zr support on the hydrogenation rate of different substrates over a Pt catalyst [30,31,33,34,50,51].

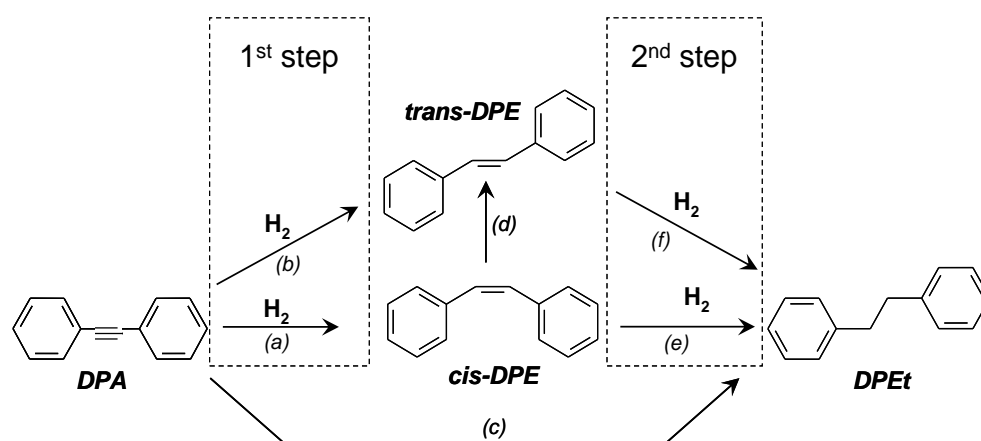


Figure 4. A two-step mechanism of DPA hydrogenation. First step—DPA to DPE hydrogenation (routes *a* and *b*). Second step—DPE to DPET hydrogenation (routes *f* and *e*). Route *c* represents the direct hydrogenation of DPA to DPET. Route *d* demonstrates *cis*- to *trans*-DPE hydro-isomerization.

Table 1. Kinetic parameters of DPA to DPE and DPE to DPET hydrogenation (first and second reaction steps, respectively) over PdAg₁₀/CZ and reference PdAg₁₀/A catalysts.

Catalyst	Calculation on the GC Data			Calculation on the Kinetic Data				
	r_1 mmol DPA (DPET) min ⁻¹ g _{cat} ⁻¹	r_2 mmol H ₂ min ⁻¹ g _{cat} ⁻¹	r_1/r_2	r_1 mmol H ₂ min ⁻¹ g _{cat} ⁻¹	r_2 mmol H ₂ min ⁻¹ g _{cat} ⁻¹	r_1/r_2	A_1 s ⁻¹	A_2 s ⁻¹
PdAg ₁₀ /CZ	4.21	0.10	37.0	4.24	0.11	39.0	1.505	0.039
PdAg ₁₀ /A	1.36	0.014	95.1	1.37	0.014	97.7	0.485	0.005

On the first reaction step, until complete DPA consumption, the yield of DPET did not exceed 1% over the reference catalyst. This is the evidence that the DPET formation through route *c* (Figure 4) is negligible, indicating the high selectivity of the catalyst toward DPE formation. The “Stilbene selectivity vs. DPA conversion” plot is displayed in Figure 3c. The selectivity of the reference catalyst was extremely high (>99%) and remained essentially constant throughout the whole DPA conversion range. This result agrees well with the previously reported one on the brilliant selectivity of SAA catalysts in partial alkyne hydrogenation [37,52–54].

It is remarkable that the selectivity of the PdAg₁₀/CZ catalyst is essentially identical to the selectivity of the reference PdAg₁₀/A (Figure 3c). The shapes of the selectivity profiles are the same for both samples, indicating high selectivity up to 100% DPA conversion.

The yields of *cis*- and *trans*-stilbenes reached a maximum after complete DPA conversion, giving 95.9% and 3.0% for the reference PdAg₁₀/A catalyst and 93.2% and 4.2% for the PdAg₁₀/CZ sample, respectively. Presumably, the formation of *cis*- and *trans*-stilbenes occurred in parallel fashion on the first reaction step. The preferential formation of the *cis*-isomer results from the syn-addition of hydrogen to the triple bond [55]. Probably, if *trans*-stilbene formation occurs in parallel to *cis*-stilbene even before the total consumption of alkyne, it is reasonable to assume that the *trans*-stilbene may be a product of direct DPA hydrogenation (route *b* on Figure 4) rather than *cis*-stilbene hydroisomerization (route *d*). However, this conclusion is tentative and requires additional detailed study.

On the second reaction step, stilbene hydrogenation leads to the formation of DPET. It is evident from the reaction profiles (Figure 3a,b) that the rate of the DPET formation (r_2) is much lower than that of the DPA consumption. Thus, over the reference PdAg₁₀/A catalyst, the r_2 value was 95 times lower compared to r_1 (Table 1, r_1/r_2). For the PdAg₁₀/CZ sample, this difference was lower (ca. 37).

It is informative to analyze the kinetic profiles of hydrogen uptake in the course of DPA hydrogenation over PdAg₁₀/A and PdAg₁₀/CZ (Figure 5). The profiles exhibit a pronounced downward bending after uptake of 1 equivalent. of H₂. It clearly indicates a decrease in the hydrogenation rate after the completion of DPA to DPE hydrogenation and a sharp slowdown in the complete hydrogenation toward alkane.

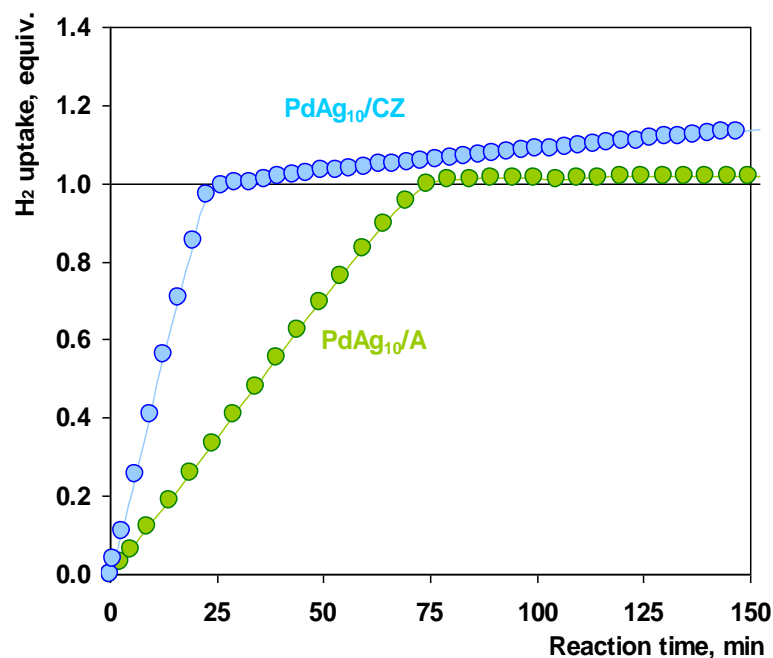


Figure 5. Kinetics of hydrogen uptake for DPA hydrogenation over SAA PdAg₁₀/A and PdAg₁₀/CZ catalysts. P(H₂) = 5 bar, m_{cat} = 10 mg, [DPA] = 1 mmol.

For both catalysts, the H₂ consumption profile on the first reaction step (DPA to DPE) was essentially linear, which suggests a close-to-zero reaction order with respect to the substrate over PdAg catalysts. This observation is consistent with previous studies on the hydrogenation of alkynes on Pd catalysts and can be explained by a much stronger adsorption of initial alkyne than reaction products [56–58].

The rates of DPA consumption and DPEt formation calculated on the basis of GC data were in good agreement with the rates of H₂ consumption (Table 1). Over the reference PdAg₁₀/A catalyst, the rate of H₂ consumption during DPA to DPE conversion was 1.37 mmol H₂ min⁻¹ g_{cat}⁻¹ and decreased extremely to 0.014 mmol H₂ min⁻¹ g_{cat}⁻¹ resulting in an r_1/r_2 ratio of ~98 (Table 1). For the PdAg₁₀/CZ catalyst, the H₂ consumption rate was significantly higher and reached 4.24 and 0.11 mmol H₂/min/g_{cat} on the first and second step, consequently resulting in an r_1/r_2 ratio of 39.

It should be noted that the stability of the catalysts under the reaction conditions is of great importance. For evaluating the possible impact of the reaction conditions on the catalyst's performance, both PdAg₁₀/A and PdAg₁₀/CZ were investigated in five repeated catalytic tests. Details of the catalytic test can be found in Section 3.5. After each hydrogenation cycle, the catalysts were recovered from the reaction mixture by centrifugation (10,000 rpm, 10 min) and washed with n-hexane to ensure removal of the reaction products from the catalyst surface, and after that, they were dried overnight. Thereafter, a new run of DPA hydrogenation was performed using the fresh solvent and reactants under the same conditions as the initial experiments. The data obtained demonstrated that the catalytic performances of the fresh catalyst and the catalyst after five catalytic cycles were essentially identical (Figures S1 and S2). This fact suggests the absence of noticeable changes in catalyst's performance in the course of DPA hydrogenation.

2.4. Discussion

Based on the experimental data, it is obvious that the activity of SAA PdAg₁₀ catalysts can be enhanced by using CeO₂–ZrO₂ as a carrier. The increase in the catalytic activity of PdAg₁₀/CZ could be attributable to both (1) change in the structure and electronic state of catalytic active sites on the surface of PdAg₁₀ nanoparticles caused by the strong metal–support interaction (SMSI) [59] and (2) change in the number of active sites.

The characterization of single-atom alloy catalysts is a challenging task. However, an analysis of the most recent reviews on this issue [40,41] allows us to identify the most efficient combination of several techniques for studying the structure of the SAA catalyst. HRTEM, EDX, DRIFTS-CO, XRD and XPS are among them. For our catalysts, the use of XPS analysis was restricted by the low Pd content. However, two powerful methods were employed for PdAg₁₀/A and PdAg₁₀/CZ analysis.

DRIFT spectroscopy of adsorbed CO is known as a simple, convenient and informative method to detect the formation of single-atom/isolated Pd₁ sites in bimetallic Pd-based structures (such as solid solutions, intermetallic phases, etc.) [40,41]. In the case of a monometallic Pd catalyst, the spectrum usually contains two main adsorption bands. The first one centered at 2100–2050 cm^{−1} corresponds to linearly bonded CO on top of the Pd atom, and the second one at 2000–1800 cm^{−1} (usually with higher intensity) is ascribed to bridged and hollow-bonded CO species on two or three neighboring Pd atoms. It should be mentioned that, on the Pd surface, multibonded CO adsorption is preferable due to higher adsorption energy (1.69–1.47 eV for hollow- and bridge-bonded CO vs. 1.15 eV for linearly adsorbed CO) [60]. On the other hand, the DRIFT spectral pattern of the PdAg SAA catalyst displayed only one band of linearly adsorbed CO, since multibonded CO adsorption on Pd₁ sites surrounded by Ag atoms is not possible [40,44,52]. The group of Prof. T. Zhang was the first to use the DRIFTS-CO technique for confirming the formation of Pd-Ag nanoparticles with an SAA structure [43], and our data agree well with those obtained by them. The DRIFTS-CO spectra of the reference PdAg₁₀/A and PdAg₁₀/CZ showed almost complete absence of multipoint CO adsorption (Figure 2). This suggests the same SAA structure of active sites for both catalysts where single Pd₁ atoms are separated from each other by Ag atoms. The similarity of electronic state of the adsorption sites for PdAg₁₀/A and PdAg₁₀/CZ also stems from the fact that the bands of linearly adsorbed CO are centered at the almost identical frequencies of 2044 and 2047 cm^{−1}, having the same symmetry and small width. Thus, the increase in catalytic activity of PdAg₁₀/CZ cannot be explained by the modification of active site properties.

The second technique for studying the structure of PdAg SAA was HRTEM. Here, we used a Themis Z advanced instrument, capable of providing EDX analysis of individual metal nanoparticles (see Section 3.3. for details). The data obtained clearly indicated that the composition of each probed nanoparticle corresponded to the Pd₁Ag₁₀, giving solid evidence of PdAg alloyed nanoparticles formation (Tables S1 and S2 for details). The HRTEM data also provided an explanation for the different catalytic activity of PdAg₁₀/CZ and PdAg₁₀/A. The most likely explanation for the higher catalytic activity of PdAg₁₀/CZ is the smaller size of the PdAg nanoparticles compared to the reference PdAg₁₀/A catalyst. Indeed, as the size of the metal particles decreases, the fraction of active metal atoms on the particle surface available for reactants increases, enhancing catalyst activity [61]. Therefore, the higher catalytic activity of the PdAg₁₀/CZ presumably stems from the formation of smaller particles with average size of 4.2 nm compared to the reference PdAg₁₀/A with relatively larger average particle size of 6.2 nm.

In turn, the decrease in the size of the PdAg nanoparticles for PdAg₁₀/CZ can be explained by the increase in the metal–support interaction energy in comparison to the PdAg₁₀/A reference catalysts. It was reported previously that the modification of CeO₂ with Zr enhances interaction between the support and metal nanoparticles, thus stabilizing small metal particles [31,62,63].

One more efficient tool to confirm PdAg alloy formation is a powder XRD. In our previous paper, we used this technique to study the structure of PdAg/ α -Al₂O₃ [44]. Owing

to the high crystallinity of α -Al₂O₃ and the relatively large size of the PdAg nanoparticles (10–12 nm), the overlap of signals of the metal nanoparticles and the support was minimized. Unfortunately, XRD is not applicable for PdAg nanoparticles supported on gamma-Al₂O₃ or CeO₂–ZrO₂ due to the smaller size of the metal particles and wide reflections of support overlapping those of Pd and Ag. Nevertheless, in the current paper we used the same preparation procedure as in [44], so we dare to hope that catalysts with the same structure were obtained. Moreover, the data from catalytic tests of PdAg₁₀/A and PdAg₁₀/CZ agree well with the previously reported results for the SAA PdAg catalyst with a Pd:Ag molar ratio of 1:3 [38,44,52].

3. Materials and Methods

3.1. Materials

Chemicals: diphenylacetylene (>98%, Sigma-Aldrich, Steinheim, Germany); *n*-hexane (98%, Merck KGaA, Darmstadt, Germany).

Metal precursors: Pd(NO₃)₂ (99.9%, 14.86% Pd, Alfa Aesar, Ward Hill, MA, USA); AgNO₃ (≥99.0%, Sigma-Aldrich, Steinheim, Germany).

Carriers for catalyst preparation: Al₂O₃ (S_{BET} = 56 m²/g, Sasol, Hamburg, Germany); 80% CeO₂–20% ZrO₂ (C20Z, S_{BET} = 102 m²/g, Ekoal'yans LLC, Novoural'sk, Russia).

Gases and gaseous mixtures: 5 vol.% H₂/Ar (MGPP LLC, Vidnoe, Moscow region, Russia); N₂ (99.999% grade, Vidnoe, Moscow region, MGPP LLC, Russia); He (99.9999% grade, Vidnoe, Moscow region, MGPP LLC, Russia); Ar (99.9999%, Balashikha, Moscow region, Linde Gas Rus, Balashikha, Moscow region, Russia); 0.5 vol.% CO/He (Balashikha, Moscow region, Linde Gas Rus, Russia).

3.2. Catalyst Preparation

Two PdAg catalysts with an identical Pd:Ag = 1:10 ratio were synthesized; the catalysts were supported on Al₂O₃ and 80% CeO₂–20% ZrO₂. The parent powder supports were precalcined in dry air flow at 500 °C for 4h. Pretreated supports were impregnated by incipient wetness co-impregnation with an aqueous solution of Pd(NO₃)₂ and AgNO₃. The impregnated materials were then treated as follows: (1) drying overnight at ambient temperature, (2) calcination at 550 °C in dry air flow (300 mL/min) and (3) reduction at 550 °C in 5 wt.% H₂/Ar flow for 3 h. After reduction, the samples were cooled down to 200 °C in 5 wt.% H₂/Ar flow. After that, the gas flow was switched from 5 wt.% H₂/Ar to N₂ of high purity, and the samples were cooled down to ambient temperature. The reduction temperature was chosen based on our previous data [38]. It has been shown that 550 °C is more than sufficient to reduce metal components and provide the required degree of mobility of Pd and Ag atoms for the formation of uniformly distributed Pd–Ag nanoparticles. According to inductively coupled plasma atomic emission spectrometry (ICP-AES) the metal content was 0.51 wt.% Pd and 5.05 wt.% Ag for Pd₁Ag₁₀/Al₂O₃ (PdAg₁₀/A) and 0.50 wt.% Pd and 5.1 wt.% Ag for Pd₁Ag₁₀/CeO₂–ZrO₂ (PdAg₁₀/CZ), which corresponds to a Pd:Ag molar ratio of 1:10.

3.3. High-Resolution Transmission Electron Microscopy

For the TEM study, all samples were ultrasonically suspended in EtOH and deposited on a holey carbon film mounted on an aluminum grid. The Themis Z instrument was used (Thermo Fisher Scientific, Eindhoven, The Netherlands). The microscope is equipped with a Ceta 16 CCD sensor, a corrector of spherical aberrations and an EDX Super-X spectrometer (Thermo Fisher Scientific, Eindhoven, The Netherlands) with a semiconductor Si detector (128 eV). The instrument operated at an accelerating voltage of 200 kV. The maximum lattice resolution was 0.07 nm.

3.4. DRIFT Spectroscopy of Adsorbed CO

The diffuse reflectance IR spectra of adsorbed CO (DRIFTS-CO) were recorded with a Tensor 27 IR instrument (Bruker, Germany) equipped with an MCT detector and a Diffuse

Reflection Catalysis Package for in situ measurements (Harrick Scientific Products, UK). Approximately 0.01–0.015 g of catalyst was placed in a CaF₂ cell and heated to 500 °C in flowing Ar with subsequent reduction in a flow of 5% H₂/Ar (30 cm³/min) at 500 °C for 1 h. Thereafter, the sample was cooled as follows: to 150 °C in a flow of 5 wt.% H₂/Ar and further to 50 °C in a flow of Ar. The background spectrum was acquired at 50 °C under Ar flow. DRIFTS-CO spectra were recorded under a flow of 0.5 vol.% CO/He (30 cm³/min) at 50 °C for 10 min (250 scans, resolution of 4 cm⁻¹).

3.5. Catalytic Tests

A batch-type reactor was used for the diphenylacetylene hydrogenation. The reaction was performed at 25 °C, under 5 bar of H₂, with 1000 rpm stirring. *n*-Hexane was chosen as a solvent. The catalytic unit was equipped with a digital pressure sensor connected to the reactor. This sensor allowed measurement of the hydrogen consumption during the reaction by recording the pressure drop. The reaction mixture was sampled and GC analyzed with a Crystal 5000 instrument (Chromatek, Russia) equipped with a flame-ionization detector. A HP5-MS GC column (30 m × 0.25 mm ID, 0.25 μm film thickness) was used to separate the products.

The H₂ consumption profile exhibited a pronounced downward bending after the consumption of 1 eq. of H₂ because alkyne hydrogenation proceeds via a two-step sequential scheme (see Figure 5). The reaction rates in mmol H₂ min⁻¹ g_{cat}⁻¹ on the 1st and 2nd reaction steps were obtained from the slope of the linear parts of the hydrogen consumption curve. Furthermore, the rates of DPA consumption (1st reaction step rate) and DPEt formation as the 2nd in mmol min⁻¹ g_{cat}⁻¹ were calculated from the time course of reaction mixture composition (Figure 3a,b) on the basis of GC analysis data. Both methods provided consistent results (Table 1).

The efficiency of the kinetic control was evaluated by comparing the rates of diphenylacetylene hydrogenation for the 1st and 2nd steps (r_1/r_2) in accordance with [64].

The specific activity normalized by Pd content on the 1st (A_1, s^{-1}) and 2nd (A_2, s^{-1}) reaction steps were calculated as follows:

$$A_n = \frac{r_n}{m_{cat} * X_{Pd} * M_{Pd} * 60}$$

Here, r_n represents the H₂ consumption rate on the 1st or 2nd reaction step in mmol H₂/min, m_{cat} and X_{Pd} represent the mass of utilized catalyst for the catalytic run and Pd content in wt.% and M_{Pd} is the molecular weight of palladium.

The selectivity toward alkene formation (S_{DPE}) was calculated based on the GC data, using the following equation:

$$S_{DPE} = \frac{n_{cis-DPE} + n_{trans-DPE}}{n_{cis-DPE} + n_{trans-DPE} + n_{DPEt}}$$

Here, $n_{cis-DPE}$ and $n_{trans-DPE}$ are the molar fractions of the *cis*- and *trans*-diphenylethylene, and n_{DPEt} is the molar fraction of diphenylethane.

Our previous experiments with different catalyst loading made it possible to eliminate gas–liquid mass transfer as the limiting factor [56]. Moreover, relying on our previous results, we ensured that the DPA hydrogenation proceeded in the kinetic regime. Thus, special precautions were taken to avoid internal and external mass-transfer limitations. It was shown [56] that, at a stirring speed exceeding 1000 rpm, identical activity and selectivity were obtained. This fact indicates the absence of external mass-transfer limitations. Internal mass-transfer limitations were minimized by carefully grinding the catalysts to obtain a fine powder with a particle size of <10 μm [65]. The Weisz–Prater criterion was used for elucidation of the mass-transfer impact [66]. When calculating the Weisz–Prater criterion for the highest reaction rate, the concentration of hydrogen in the solvent, the effective diffusion coefficient of hydrogen and a ratio of porosity to tortuosity of 0.1 were taken

into account. The calculation gives a Weiss–Prater value of <0.02 , indicating that internal mass-transfer limitations can be eliminated.

4. Conclusions

In this work, we investigated the effects of the support on the properties of PdAg/Al₂O₃ and PdAg/CeO₂–ZrO₂ catalysts in hydrogenation of DPA. Both catalysts with a Ag/Pd molar ratio of 10 were obtained via the incipient wet impregnation technique. The structure of the catalysts was studied using HRTEM and DRIFTS-CO. The formation of SAA nanoparticles was supported by STEM-EDX spectrum imaging. The DRIFTS-CO data confirm that the formation of single-atom Pd₁ sites isolated from each other by Ag atoms occurs on the surface of supported bimetallic Pd–Ag nanoparticles for both catalysts. According to catalytic data, the use of a CeO₂–ZrO₂ support significantly enhanced the activity of SAA PdAg catalysts in DPA hydrogenation while maintaining extremely high target selectivity within the entire DPA conversion range. The high selectivity of the PdAg/CeO₂–ZrO₂ catalyst was retained due to its high dispersion compared to PdAg/Al₂O₃, as evidenced by the HRTEM data.

Supplementary Materials: The following supporting information can be downloaded at: <https://www.mdpi.com/article/10.3390/inorganics11040150/s1>, Figure S1: EDX spectrum of PdAg₁₀/CZ (a) and PdAg₁₀/A (b) catalysts.; Figure S2: Products distribution of DPA hydrogenation over PdAg₁₀/A (a) and PdAg₁₀/CZ (b) after 1st and 5th reaction runs; Figure S3: Comparison of selectivity toward stilbene formation for PdAg₁₀/A and PdAg₁₀/CZ catalysts after 1st and 5th reaction runs; Table S1: Quantitative analysis of EDX-spectrum of PdAg₁₀/CZ catalyst; Table S2. Quantitative analysis of EDX-spectrum of PdAg₁₀/A catalyst.

Author Contributions: Conceptualization: A.Y.S., I.S.M., A.V.B. and Y.V.Z.; methodology: A.Y.S. and A.V.B.; validation: P.V.M., N.S.S., G.N.B., G.O.B., A.V.B. and E.Y.G.; formal analysis: P.V.M., N.S.S., G.N.B., G.O.B., A.V.B. and E.Y.G.; investigation: P.V.M., N.S.S., G.N.B., G.O.B., A.V.B. and E.Y.G.; resources: G.N.B. and G.O.B.; data curation: A.V.B. and I.S.M.; writing—original draft preparation: P.V.M., N.S.S., G.O.B. and I.S.M.; writing—review and editing: A.Y.S., I.S.M., A.V.B. and Y.V.Z.; visualization: I.S.M. and P.V.M.; supervision: A.Y.S. and Y.V.Z.; project administration: A.Y.S. and Y.V.Z. All authors have read and agreed to the published version of the manuscript.

Funding: This work was supported by the Russian Science Foundation (grant No. 19-13-00285-P).

Institutional Review Board Statement: Not applicable.

Informed Consent Statement: Not applicable.

Data Availability Statement: All the reported data were taken from the published materials referenced below.

Conflicts of Interest: The authors declare no conflict of interest.

References

1. Jiang, K.; Pinchuk, A.O. Noble Metal Nanomaterials: Synthetic Routes, Fundamental Properties, and Promising Applications. *Solid State Phys.* **2015**, *66*, 131–211.
2. Ludwig, J.R.; Schindler, C.S. Catalyst: Sustainable Catalysis. *Chemistry* **2017**, *2*, 313–316. [[CrossRef](#)]
3. Patil, K.N.; Manikanta, P.; Srinivasappa, P.M.; Jadhav, A.H.; Nagaraja, B.M. State-of-the-art and perspectives in transition metal-based heterogeneous catalysis for selective hydrogenation of cinnamaldehyde. *J. Environ. Chem. Eng.* **2023**, *11*, 109168. [[CrossRef](#)]
4. Xu, Y.; Zhang, X.; Liu, Y.; Wang, R.; Yang, Y.; Chen, J. A critical review of research progress for metal alloy materials in hydrogen evolution and oxygen evolution reaction. *Environ. Sci. Pollut. Res.* **2022**, *30*, 11302–11320. [[CrossRef](#)]
5. Zhao, X.; Chang, Y.; Chen, W.-J.; Wu, Q.; Pan, X.; Chen, K.; Weng, B. Recent Progress in Pd-Based Nanocatalysts for Selective Hydrogenation. *ACS Omega* **2022**, *7*, 17–31. [[CrossRef](#)] [[PubMed](#)]
6. Glyzdova, D.V.; Smirnova, N.S.; Shlyapin, D.A.; Tsyru'nikov, P.G. Gas-Phase and Liquid-Phase Hydrogenation of Acetylene in Lean and Enriched Mixtures over Supported Modified Palladium Catalysts. *Russ. J. Gen. Chem.* **2020**, *90*, 1120–1140. [[CrossRef](#)]
7. Shittu, T.D.; Ayodele, O.B. Catalysis of semihydrogenation of acetylene to ethylene: Current trends, challenges, and outlook. *Front. Chem. Sci. Eng.* **2022**, *16*, 1031–1059. [[CrossRef](#)]

8. Chen, X.; Shi, C.; Liang, C. Highly selective catalysts for the hydrogenation of alkynols: A review. *Chin. J. Catal.* **2021**, *42*, 2105–2121. [[CrossRef](#)]
9. Deng, X.; Wang, J.; Guan, N.; Li, L. Catalysts and mechanisms for the selective heterogeneous hydrogenation of carbon-carbon triple bonds. *Cell Rep. Phys. Sci.* **2022**, *3*, 101017. [[CrossRef](#)]
10. Li, H.; Li, L.; Li, Y. The electronic structure and geometric structure of nanoclusters as catalytic active sites. *Nanotechnol. Rev.* **2013**, *2*, 515–528. [[CrossRef](#)]
11. Hannagan, R.T.; Giannakakis, G.; Flytzani-Stephanopoulos, M.; Sykes, E.C.H. Single-Atom Alloy Catalysis. *Chem. Rev.* **2020**, *120*, 12044–12088. [[CrossRef](#)] [[PubMed](#)]
12. Han, J.; Lu, J.; Wang, M.; Wang, Y.; Wang, F. Single Atom Alloy Preparation and Applications in Heterogeneous Catalysis. *Chin. J. Chem.* **2019**, *37*, 977–988. [[CrossRef](#)]
13. Mao, J.; Yin, J.; Pei, J.; Wang, D.; Li, Y. Single atom alloy: An emerging atomic site material for catalytic applications. *Nano Today* **2020**, *34*, 100917. [[CrossRef](#)]
14. Ciriminna, R.; Ghahremani, M.; Karimi, B.; Pagliaro, M.; Luque, R. Single-atom catalysis: A practically viable technology? *Curr. Opin. Green Sustain. Chem.* **2020**, *25*, 100358. [[CrossRef](#)]
15. Wang, K.; Li, G.; Wu, C.; Sui, X.; Wang, Q.; He, J. Effects of Ag Atomic Segregation from Different Planes on the Size-Dependent Melting of Ag–Pd Clusters. *J. Cluster Sci.* **2016**, *27*, 55–62. [[CrossRef](#)]
16. Okhlopko, L.B.; Cherepanova, S.V.; Prosvirin, I.P.; Kerzhentsev, M.A.; Ismagilov, Z.R. Semihydrogenation of 2-methyl-3-butyn-2-ol on Pd–Zn nanoalloys: Effect of composition and heterogenization. *Appl. Catal. A General* **2018**, *549*, 245–253. [[CrossRef](#)]
17. Concepción, P.; García, S.; Hernández-Garrido, J.C.; Calvino, J.J.; Corma, A. A promoting effect of dilution of Pd sites due to gold surface segregation under reaction conditions on supported Pd–Au catalysts for the selective hydrogenation of 1,5-cyclooctadiene. *Catal. Today* **2016**, *259*, 213–221. [[CrossRef](#)]
18. Shesterkina, A.A.; Kirichenko, O.A.; Kozlova, L.M.; Kapustin, G.I.; Mishin, I.V.; Strelkova, A.A.; Kustov, L.M. Liquid-phase hydrogenation of phenylacetylene to styrene on silica-supported Pd–Fe nanoparticles. *Mendeleev Commun.* **2016**, *26*, 228–230. [[CrossRef](#)]
19. Marcinkowski, M.D.; Liu, J.; Murphy, C.J.; Liriano, M.L.; Wasio, N.A.; Lucci, F.R.; Flytzani-Stephanopoulos, M.; Sykes, E.C.H. Selective Formic Acid Dehydrogenation on Pt–Cu Single-Atom Alloys. *ACS Catal.* **2016**, *7*, 413–420. [[CrossRef](#)]
20. Lucci, F.R.; Liu, J.; Marcinkowski, M.D.; Yang, M.; Allard, L.F.; Flytzani-Stephanopoulos, M.; Sykes, E.C.H. Selective hydrogenation of 1,3-butadiene on platinum-copper alloys at the single-atom limit. *Nat. Commun.* **2015**, *6*, 8550. [[CrossRef](#)]
21. Kyriakou, G.; Boucher, M.B.; Jewell, A.D.; Lewis, E.A.; Lawton, T.J.; Baber, A.E.; Tierney, H.L.; Flytzani-Stephanopoulos, M.; Sykes, E.C.H. Isolated metal atom geometries as a strategy for selective heterogeneous hydrogenations. *Science* **2012**, *335*, 1209–1212. [[CrossRef](#)]
22. Abdel-Mageed, A.M.; Chen, S.; Fauth, C.; Häring, T.; Bansmann, J. Fundamental Aspects of Ceria Supported Au Catalysts Probed by In Situ/Operando Spectroscopy and TAP Reactor Studies. *ChemPhysChem* **2021**, *22*, 1302–1315. [[CrossRef](#)] [[PubMed](#)]
23. Schubert, M.M.; Hackenberg, S.; van Veen, A.C.; Muhler, M.; Plzak, V.; Jürgen Behm, R. CO Oxidation over Supported Gold Catalysts—“Inert” and “Active” Support Materials and Their Role for the Oxygen Supply during Reaction. *J. Catal.* **2001**, *197*, 113–122. [[CrossRef](#)]
24. Razmgar, K.; Altarawneh, M.; Oluwoye, I.; Senanayake, G. Ceria-Based Catalysts for Selective Hydrogenation Reactions: A Critical Review. *Catal. Surv. Asia* **2021**, *25*, 27–47. [[CrossRef](#)]
25. Anand, S.; Pinheiro, D.; Sunaja Devi, K.R. Recent Advances in Hydrogenation Reactions Using Bimetallic Nanocatalysts: A Review. *Asian J. Org. Chem.* **2021**, *10*, 3068. [[CrossRef](#)]
26. Nelson, N.C.; Manzano, J.S.; Sadow, A.D.; Overbury, S.H.; Slowing, I.I. Selective Hydrogenation of Phenol Catalyzed by Palladium on High-Surface-Area Ceria at Room Temperature and Ambient Pressure. *ACS Catal.* **2015**, *5*, 2051–2061. [[CrossRef](#)]
27. Velu, S.; Kapoor, M.P.; Inagaki, S.; Suzuki, K. Vapor phase hydrogenation of phenol over palladium supported on mesoporous CeO₂ and ZrO₂. *Appl. Catal. A General* **2003**, *245*, 317–331. [[CrossRef](#)]
28. Teng, M.; Luo, L.; Yang, X. Synthesis of mesoporous Ce_{1-x}Zr_xO₂ (x = 0.2–0.5) and catalytic properties of CuO based catalysts. *Microporous Mesoporous Mater.* **2009**, *119*, 158–164. [[CrossRef](#)]
29. Zhang, X.; Wang, Q.; Zhang, J.; Wang, J.; Guo, M.; Chen, S.; Li, C.; Hu, C.; Xie, Y. One step hydrothermal synthesis of CeO₂–ZrO₂ nanocomposites and investigation of the morphological evolution. *RSC Adv.* **2015**, *5*, 89976–89984. [[CrossRef](#)]
30. Bhogeswararao, S.; Srinivas, D. Intramolecular selective hydrogenation of cinnamaldehyde over CeO₂–ZrO₂-supported Pt catalysts. *J. Catal.* **2012**, *285*, 31–40. [[CrossRef](#)]
31. Wei, S.; Zhao, Y.; Fan, G.; Yang, L.; Li, F. Structure-dependent selective hydrogenation of cinnamaldehyde over high-surface-area CeO₂–ZrO₂ composites supported Pt nanoparticles. *Chem. Eng. J.* **2017**, *322*, 234–245. [[CrossRef](#)]
32. Bhogeswararao, S.; Srinivas, D. Chemoselective Hydrogenation of Cinnamaldehyde over Pd/CeO₂–ZrO₂ Catalysts. *Catal. Lett.* **2010**, *140*, 55–64. [[CrossRef](#)]
33. Vikanova, K.V.; Redina, E.A.; Kapustin, G.I.; Davshan, N.A.; Kustov, L.M. Hydrogenation of Acetophenone at Room Temperature and Atmospheric Pressure over Pt-Containing Catalysts Supported on Reducible Oxides. *Russ. J. Phys. Chem. A* **2019**, *93*, 231–235. [[CrossRef](#)]

34. Redina, E.A.; Vikanova, K.V.; Kapustin, G.I.; Mishin, I.V.; Tkachenko, O.P.; Kustov, L.M. Selective Room-Temperature Hydrogenation of Carbonyl Compounds under Atmospheric Pressure over Platinum Nanoparticles Supported on Ceria-Zirconia Mixed Oxide. *Eur. J. Org. Chem.* **2019**, *2019*, 4159–4170. [[CrossRef](#)]
35. Redina, E.A.; Vikanova, K.V. Highly Efficient Pt-Catalyst Supported on Mesoporous Ceria-Zirconia Oxide for Hydrogenation of Nitroaromatic Compounds to Anilines. *Russ. J. Phys. Chem. A* **2018**, *92*, 2374–2378. [[CrossRef](#)]
36. Vikanova, K.V.; Redina, E.A. Influence of the Specific Surface Area of CeO₂-ZrO₂ Supports on the Activity of Pt-Containing Catalysts in the Cinnamaldehyde Hydrogenation Reaction. *Russ. J. Phys. Chem. A* **2018**, *92*, 2355–2358. [[CrossRef](#)]
37. Rassolov, A.V.; Mashkovsky, I.S.; Baeva, G.N.; Bragina, G.O.; Smirnova, N.S.; Markov, P.V.; Bukhtiyarov, A.V.; Wärnå, J.; Stakheev, A.Y.; Murzin, D.Y. Liquid-Phase Hydrogenation of 1-Phenyl-1-propyne on the Pd₁Ag₃/Al₂O₃ Single-Atom Alloy Catalyst: Kinetic Modeling and the Reaction Mechanism. *Nanomaterials* **2021**, *11*, 3286. [[CrossRef](#)]
38. Rassolov, A.V.; Bragina, G.O.; Baeva, G.N.; Mashkovsky, I.S.; Stakheev, A.Y. Alumina-Supported Palladium-Silver Bimetallic Catalysts with Single-Atom Pd₁ Sites in the Liquid-Phase Hydrogenation of Substituted Alkynes. *Kinet. Catal.* **2020**, *61*, 869–878. [[CrossRef](#)]
39. Rassolov, A.V.; Bragina, G.O.; Baeva, G.N.; Mashkovsky, I.S.; Smirnova, N.S.; Gerasimov, E.Y.; Bukhtiyarov, A.V.; Zubavichus, Y.V.; Stakheev, A.Y. Highly Active Bimetallic Single-Atom Alloy PdAg Catalysts on Cerium-Containing Supports in the Hydrogenation of Alkynes to Alkenes. *Kinet. Catal.* **2022**, *63*, 756–764. [[CrossRef](#)]
40. Meunier, F.C. Relevance of IR Spectroscopy of Adsorbed CO for the Characterization of Heterogeneous Catalysts Containing Isolated Atoms. *J. Phys. Chem. C* **2021**, *125*, 21810–21823. [[CrossRef](#)]
41. Li, X.; Yang, X.; Zhang, J.; Huang, Y.; Liu, B. In Situ/Operando Techniques for Characterization of Single-Atom Catalysts. *ACS Catal.* **2019**, *9*, 2521–2531. [[CrossRef](#)]
42. Kovnir, K.; Armbrüster, M.; Teschner, D.; Venkov, T.V.; Jentoft, F.C.; Knop-Gericke, A.; Grin, Y.; Schlögl, R. A new approach to well-defined, stable and site-isolated catalysts. *Sci. Technol. Adv. Mater.* **2007**, *8*, 420–427. [[CrossRef](#)]
43. Pei, G.H.; Liu, X.Y.; Wang, A.; Lee, A.F.; Isaacs, M.A.; Li, L.; Pan, X.; Yang, X.; Wang, X.; Tai, Z.; et al. Ag Alloyed Pd Single-Atom Catalysts for Efficient Selective Hydrogenation of Acetylene to Ethylene in Excess Ethylene. *ACS Catal.* **2015**, *5*, 3717–3725. [[CrossRef](#)]
44. Rassolov, A.V.; Bragina, G.O.; Baeva, G.N.; Smirnova, N.S.; Kazakov, A.V.; Mashkovsky, I.S.; Bukhtiyarov, A.V.; Zubavichus, Y.V.; Stakheev, A.Y. Formation of Isolated Single-Atom Pd₁ Sites on the Surface of Pd-Ag/Al₂O₃ Bimetallic Catalysts. *Kinet. Catal.* **2020**, *61*, 758–767. [[CrossRef](#)]
45. Rassolov, A.V.; Bragina, G.O.; Baeva, G.N.; Smirnova, N.S.; Kazakov, A.V.; Mashkovsky, I.S.; Stakheev, A.Y. Liquid-Phase Hydrogenation of Internal and Terminal Alkynes on Pd-Ag/Al₂O₃ Catalyst. *Kinet. Catal.* **2019**, *60*, 642–649. [[CrossRef](#)]
46. Primet, M.; Mathieu, M.V.; Sachtler, W.M.H. Infrared Spectra of Carbon Monoxide Adsorbed on Silica-Supported PdAg Alloys. *J. Catal.* **1976**, *44*, 324–327. [[CrossRef](#)]
47. Lear, T.; Marshall, R.; Lopez-Sanchez, J.A.; Jackson, S.D.; Klapotke, T.M.; Baumer, M.; Rupprechter, G.; Freund, H.-J.; Lennon, D. The application of infrared spectroscopy to probe the surface morphology of alumina-supported palladium catalysts. *J. Chem. Phys.* **2005**, *123*, 174706. [[CrossRef](#)]
48. Markov, P.V.; Mashkovsky, I.S.; Baeva, G.N.; Stakheev, A.Y. Hydroisomerization of cis-Stilbene into trans-Stilbene on Supported Heterogeneous Metal Catalysts (Rh, Pd, Pt, Ru, Ir/ α -Al₂O₃). *Kinet. Catal.* **2017**, *58*, 771–779. [[CrossRef](#)]
49. Markov, P.V.; Smirnova, N.S.; Baeva, G.N.; Bukhtiyarov, A.V.; Mashkovsky, I.S.; Stakheev, A.Y. Intermetallic Pd_xIn_y/Al₂O₃ catalysts with isolated single-atom Pd sites for one-pot hydrogenation of diphenylacetylene into trans-stilbene. *Mendeleev Commun.* **2020**, *30*, 468–471. [[CrossRef](#)]
50. Reddy, B.M.; Rao, K.N.; Reddy, G.K. Controlled Hydrogenation of Acetophenone Over Pt/CeO₂-MO_x (M = Si, Ti, Al, and Zr) Catalysts. *Catal. Lett.* **2009**, *131*, 328–336. [[CrossRef](#)]
51. Serrano-Ruiz, J.C.; Luettich, J.; Sepúlveda-Escribano, A.; Rodríguez-Reinoso, F. Effect of the support composition on the vapor-phase hydrogenation of crotonaldehyde over Pt/Ce_xZr_{1-x}O₂ catalysts. *J. Catal.* **2006**, *241*, 45–55. [[CrossRef](#)]
52. Rassolov, A.V.; Mashkovsky, I.S.; Bragina, G.O.; Baeva, G.N.; Markov, P.V.; Smirnova, N.S.; Wärnå, J.; Stakheev, A.Y.; Murzin, D.Y. Kinetics of liquid-phase diphenylacetylene hydrogenation on “single-atom alloy” Pd-Ag catalyst: Experimental study and kinetic analysis. *Mol. Catal.* **2021**, *506*, 111550. [[CrossRef](#)]
53. Giannakakis, G.; Flytzani-Stephanopoulos, M.; Sykes, E.C.H. Single-Atom Alloys as a Reductionist Approach to the Rational Design of Heterogeneous Catalysts. *Acc. Chem. Res.* **2019**, *52*, 237–247. [[CrossRef](#)] [[PubMed](#)]
54. Liu, J.; Uhlman, M.B.; Montemore, M.M.; Trimpalis, A.; Giannakakis, G.; Shan, J.; Cao, S.; Hannagan, R.T.; Sykes, E.C.H.; Flytzani-Stephanopoulos, M. Integrated Catalysis-Surface Science-Theory Approach to Understand Selectivity in the Hydrogenation of 1-Hexyne to 1-Hexene on PdAu Single-Atom Alloy Catalysts. *ACS Catal.* **2019**, *9*, 8757–8765. [[CrossRef](#)]
55. Chen, B.; Dingerdissen, U.; Krauter, J.G.E.; Lansink Rotgerink, H.G.J.; Möbus, K.; Ostgard, D.J.; Panster, P.; Riermeier, T.H.; Seebald, S.; Tacke, T.; et al. New developments in hydrogenation catalysis particularly in synthesis of fine and intermediate chemicals. *Appl. Catal. A General* **2005**, *280*, 17–46. [[CrossRef](#)]
56. Markov, P.V.; Bragina, G.O.; Baeva, G.N.; Tkachenko, O.P.; Mashkovsky, I.S.; Yakushev, I.A.; Kozitsyna, N.Y.; Vargaftik, M.N.; Stakheev, A.Y. Pd-Cu Catalysts from Acetate Complexes in Liquid Phase Diphenylacetylene Hydrogenation. *Kinet. Catal.* **2015**, *56*, 591–597. [[CrossRef](#)]

57. Markov, P.V.; Mashkovsky, I.S.; Bragina, G.O.; Wärnå, J.; Gerasimov, E.Y.; Bukhtiyarov, V.I.; Stakheev, A.Y.; Murzin, D.Y. Particle size effect in liquid-phase hydrogenation of phenylacetylene over Pd catalysts: Experimental data and theoretical analysis. *Chem. Eng. J.* **2019**, *35.8*, 520–530. [[CrossRef](#)]
58. Markov, P.V.; Mashkovsky, I.S.; Bragina, G.O.; Wärnå, J.; Bukhtiyarov, V.I.; Stakheev, A.Y.; Murzin, D.Y. Experimental and theoretical analysis of particle size effect in liquid-phase hydrogenation of diphenylacetylene. *Chem. Eng. J.* **2021**, *404*, 126409. [[CrossRef](#)]
59. Stakheev, A.Y.; Kustov, L.M. Effects of the support on the morphology and electronic properties of supported metal clusters: Modern concepts and progress in 1990s. *Appl. Catal. A* **1999**, *188*, 3–35. [[CrossRef](#)]
60. Yudanov, I.V.; Sahnoun, R.; Neyman, K.M.; Rösch, N.; Hoffmann, J.; Schauermaun, S.; Johánek, V.; Unterhalt, H.; Rupprechter, G.; Libuda, J.; et al. CO Adsorption on Pd Nanoparticles: Density Functional and Vibrational Spectroscopy Studies. *J. Phys. Chem. B* **2003**, *107*, 255–264. [[CrossRef](#)]
61. Nikolaev, S.A.; Zhanaveskin, L.N.; Smirnov, V.V.; Aver'yanov, V.A.; Zhanaveskin, K.L. Catalytic hydrogenation of alkyne and alkadiene impurities in alkenes. Practical and theoretical aspects. *Russ. Chem. Rev.* **2009**, *78*, 231–247. [[CrossRef](#)]
62. Alifanti, M.; Baps, B.; Blangenois, N.; Naud, J.; Grange, P.; Delmon, B. Characterization of CeO₂–ZrO₂ Mixed Oxides. Comparison of the Citrate and Sol-Gel Preparation Methods. *Chem. Mater.* **2003**, *15*, 395–403. [[CrossRef](#)]
63. Liang, Q.; Wu, X.; Wu, X.; Weng, D. Role of Surface Area in Oxygen Storage Capacity of Ceria–Zirconia as Soot Combustion Catalyst. *Catal. Lett.* **2007**, *119*, 265–270. [[CrossRef](#)]
64. Spee, M.P.R.; Boersma, J.; Meijer, M.D.; Slagt, M.Q.; van Koten, G.; Geus, J.W. Selective Liquid-Phase Semihydrogenation of Functionalized Acetylenes and Propargylic Alcohols with Silica-Supported Bimetallic Palladium-Copper Catalysts. *J. Org. Chem.* **2001**, *66*, 1647–1656. [[CrossRef](#)] [[PubMed](#)]
65. Ramachandran, P.A.; Chaudhari, R.V. *Three-Phase Catalytic Reactors*; Gordon and Breach: Philadelphia, PA, USA, 1983; p. 32.
66. Weisz, P.B.; Prater, C.D. Interpretation of Measurements in Experimental Catalysis. *Adv. Catal.* **1954**, *6*, 143–196.

Disclaimer/Publisher's Note: The statements, opinions and data contained in all publications are solely those of the individual author(s) and contributor(s) and not of MDPI and/or the editor(s). MDPI and/or the editor(s) disclaim responsibility for any injury to people or property resulting from any ideas, methods, instructions or products referred to in the content.